Microscopy study of biologically mediated alteration of natural mid-oceanic ridge basalts and magnetic implications

Julie Carlut, Karim Benzerara, Hélène Horen, Nicolas Menguy, Dominique Janots, Nathaniel Findling, Amhed Addad, Imène Machouk

Microscopy study of biologically mediated alteration of natural mid-oceanic ridge basalts and magnetic implications

Julie Carlut,[1] Karim Benzerara,[2] Hélène Horen,[3] Nicolas Menguy,[2] Dominique Janots,[1] Nathaniel Findling,[1] Amhed Addad,[4] and Imène Machouk[2]

Received 28 August 2009; revised 24 February 2010; accepted 16 July 2010; published 14 October 2010.

[1] Microbial communities have been shown over the last few years to be a significant component of the subseafloor crustal environment. However, their role in the low-temperature alteration of seafloor basalts remains an open question. Among the diversity of microorganisms that can contribute to oceanic rock weathering, sulfate-reducing bacteria have been suggested, based on sulfur isotope studies, to be major actors. Previous laboratory experiments conducted on basalt samples from the Juan de Fuca Ridge incubated with model sulfate-reducing bacteria for several months showed that bacterial activity can play a role in the decrease of seafloor magnetic signal. In this paper, we characterized alteration features at the nanoscale in one of these basalt samples in order to better understand the mechanisms of the magnetic signal decrease. For that purpose, we used a combination of focused ion beam milling, transmission electron microscopy and scanning transmission X-ray microscopy. Fossilized microbial cells and phyllosilicates were evidenced at the surface of the sample. Within the sample, alteration rims mostly composed of Fe and S and measuring 100–300 nm in thickness were observed around titanomagnetites crystals that bear most of the magnetic signal. In contrast, these features were not observed on noninoculated control samples. This study offers a detailed view of the specific mineral assemblages formed in the presence of model sulfate-reducing bacteria that can be looked for in the oceanic crust. These observations contribute to understand the potential role of microbes in the alteration of the oceanic crust.

Citation: Carlut, J., K. Benzerara, H. Horen, N. Menguy, D. Janots, N. Findling, A. Addad, and I. Machouk (2010), Microscopy study of biologically mediated alteration of natural mid-oceanic ridge basalts and magnetic implications, *J. Geophys. Res.*, *115*, G00G11, doi:10.1029/2009JG001139.

1. Introduction: Objectives

[2] The presence of microorganisms in deep-sea environments and within the oceanic crust has been attested by several studies [e.g., *Thorseth et al.*, 1995, 2001; *Edwards et al.*, 2005; *Lysnes et al.*, 2004; *Templeton et al.*, 2005; *Huber et al.*, 2006; *Santelli et al.*, 2008]. Microorganisms are thought to play a role in the alteration of the crust by modifying the nearby environment via their metabolic activity [*Fisk et al.*, 1998; *Staudigel et al.*, 2008; *Edwards et al.*, 2004]. The significance of this role, its geochemical impact as well as the potential bio-signatures left by the microbes within the weathering products are, however, still not well understood. This is partly due to the technical difficulty to perform direct in situ analyses of bacterial activity and to monitor the chemical reactions that are involved. Contamination of samples and unrepresentative sampling are also important issues when dealing with retrieved material from deep sea locations. An alternative approach to test whether specific bacteria species may have an impact on the properties of seafloor rocks, is to setup experiments in the laboratory.

[3] Among the different mineral phases composing seafloor rocks, iron-bearing minerals and their weathering products are of particular interest. Due to its valence, iron is indeed very sensitive to changes in oxygen fugacity conditions. Moreover, changes in valence induce changes in mobility, Fe^{2+}, the reduced form, being usually more mobile than Fe^{3+} in aqueous environment. Finally, chemical modifications of iron-bearing phases impact the bulk magnetic properties of seafloor basalts. Hence the magnetic signal can be used as a very sensitive indicator of iron oxide transformations [e.g., *Aubourg et al.*, 2008]. The major iron oxide carrying the magnetic signal within the upper oceanic crust is titanomagnetite and its oxidized form titanomaghemite [see, e.g., *Dunlop and Ozdemir*, 1997]. In a previous study [*Carlut*

[1]Laboratoire de Géologie, UMR 8538, Ecole Normale Supérieure, CNRS, Paris, France.
[2]Equipe Géobiosphère Actuelle et Primitive, UMR 7590, Institut de Minéralogie et de Physique des Milieux Condensés, CNRS, Universités Paris 6 et 7 and IPGP 140, Paris, France.
[3]Département de Géologie, Université de Picardie Jules Verne, Amiens, France.
[4]Laboratoire de Structure et Propriétés de l'Etat Solide, UMR-CNRS 8008, Bât. C6 - Cité Scientifique, Université des Sciences et Technologies de Lille, Villeneuve d'Ascq, France.

0148-0227/10/2009JG001139

et al., 2007], very recent ("zero age") natural Mid Oceanic Ridge Basalt (MORB) samples were incubated in the laboratory with sulfate-reducing *Desulfovibrio profundus* cells [*Bale et al.*, 1997]. Sulfate-reducing bacteria (SRB) have indeed been shown to be widespread in diverse subseafloor environments as sediments [e.g., *Coleman et al.*, 1993; *Ravenschlag et al.*, 1999] young and aging ocean crust [e.g., *Huber et al.*, 2006; *Cowen et al.*, 2003] or black smokers [*Zhou et al.*, 2009]. This metabolism uses sulfate to oxidize organic matter and produces sulfide as a by-product. It was showed in [*Carlut et al.*, 2007] that SRB activity causes a drop in magnetization in young oceanic basalts. The positive correlation between bacteria activity and magnetization loss led us to search for alteration features of the titanomagnetites in the samples. A change in bulk magnetization of the samples is indeed the hallmark of a change in the composition or structure of the magnetic phases. Little evidences of such changes were found using scanning electron microscopy and rock magnetic techniques in the work of *Carlut et al.* [2007]. The goal of the present study is thus to use more appropriate analytical techniques to understand by which mechanism bacterial activity alters titanomagnetite composition or structure. This question is central in order to understand how bacteria may play an active role in an early stage of the magnetic alteration of the oceanic crust and be responsible of a change in this geophysical signal. Two main questions are therefore addressed in this paper: (1) What can we learn on the chemical composition and structure of biologically altered magnetic phases using nanoscale microscopy techniques? (2) Can we describe how microbial cells involved in this process look like and determine if they are spatially associated with alteration phases?

[4] In the present study, we adress these questions using focused ion beam (FIB) milling, transmission electron microscopy (TEM) and synchrotron-based scanning transmission X-ray microscopy (STXM). The chemistry and mineralogy of MORB samples incubated in the presence of SRB and showing a decrease in magnetization are characterized. Results from a control sample kept under sterile conditions are also reported for comparison. We show that titanomanetites are significantly altered at the micron scale under the action of SRB. Furthermore it has been possible to describe the weathering products and bacterium-mineral interfaces down to the few nm scale. As a result, we discuss the nature of the phases resulting from the weathering of magnetic minerals and the geophysical implications.

2. Material

[5] A series of 16 in-vitro experiments were reported in [*Carlut et al.*, 2007], including fresh basalt samples from mid oceanic ridges (MORB) incubated with SRB and abiotic control experiments in which fresh basalt samples were incubated in the same culture medium but kept sterile. We summarize here briefly the experimental procedure that was used and the main results. Details about the magnetic monitoring performed during the incubation of these samples during several months are given by *Carlut et al.* [2007].

2.1. Growth Condition

[6] Seawater filtered, autoclaved, degassed with argon and reduced with buffered 0.4% Na_2S was used as the medium for all experiments. This solution was then supplemented with lactate at 0.3%. No vitamins or other supplements were provided. The basalt samples were approximately 1 cm^3 in size and were immersed in flasks containing 15 ml of the medium. The 5 ml flask headspace was filled with Argon. Temperature was maintained at 28°C and flasks were not agitated. Eight flasks were inoculated with SRB while 8 served as controls. Five ml of the medium were removed sterilely every two weeks and replaced by fresh growth medium to maintain the cultures metabolically active for an extended period. The bulk remanent magnetization of the sample was monitored by regular measurements of the flasks in a cryogenic 2G magnetometer in order to detect a possible alteration of iron-bearing phases. Results showed a loss of magnetization for the samples in a biotic environment; in contrast, no magnetization loss or gain was observed for control samples immersed in the same but sterile solution (all these results are reported by *Carlut et al.* [2007]). In addition to magnetization monitoring, pH and the number of cells were followed all along the experiment. Evidence for the absence of oxygen is given indirectly by the observation that *Desulfovibrio profundus* was growing although it is strictly anaerobe [*Bale et al.*, 1997]. Results showed a rapid decrease of pH from 7.5 to 6.6–6.9 then stabilization around these pH values in both biotic and abiotic control flasks. The number of bacteria in biotic flasks was stable in the order of 10^6 cells/ml.

2.2. Selected Samples

[7] Two samples from this study were selected here: samples AnF-A and AnF-B. Both come from the inner part of a very recent (few years to a few tens of years) lobate flow piece recovered along the Juan de Fuca ridge in 1999 [*Johnson et al.*, 2002] and named Animal farm (AnF in the following). Sample AnF-B is a control sample incubated in the culture solution but kept under abiotic conditions, while sample AnF-A was immersed in a solution inoculated with *Desulfovibrio profundus* (DSMZ, #11384) belonging to the delta subclass of *Proteobacteria* and able to use sulfate (and possibly ferric iron) as electron acceptor for growth [*Bale et al.*, 1997]. Previous rock magnetic studies made on these samples showed that the magnetic carriers are pseudo single-domain titanomagnetites [*Carlut and Kent*, 2002]. The loss of magnetization in sample AnF-A after 142 days was on the order of 10%, while no changes were noticeable on the control AnF-B sample. Both samples were subsequently retrieved from the flasks and observed by Scanning Electron Microscopy (SEM). SEM observations revealed significant differences between the control and the sample incubated with bacteria. Sharp surfaces were observed in the control sample, whereas numerous phyllosilicates, as well as filaments were observed in the sample inoculated with bacteria. Each filament was of constant diameter, i.e., between 1 and 2 μm but their overall length was variable reaching sometimes a few tens of microns. Energy dispersive X-ray spectrometry (EDXS) analyses performed by SEM revealed the presence of Fe and S within the filaments. The diameter of the filaments, close to the diameter of *Desulfovibrio profundus* bacteria, and their chemical composition suggested that filaments may represent cells encrusted by minerals but no firm conclusion could be drawn. In addition to these observations semiquantitative EDXS

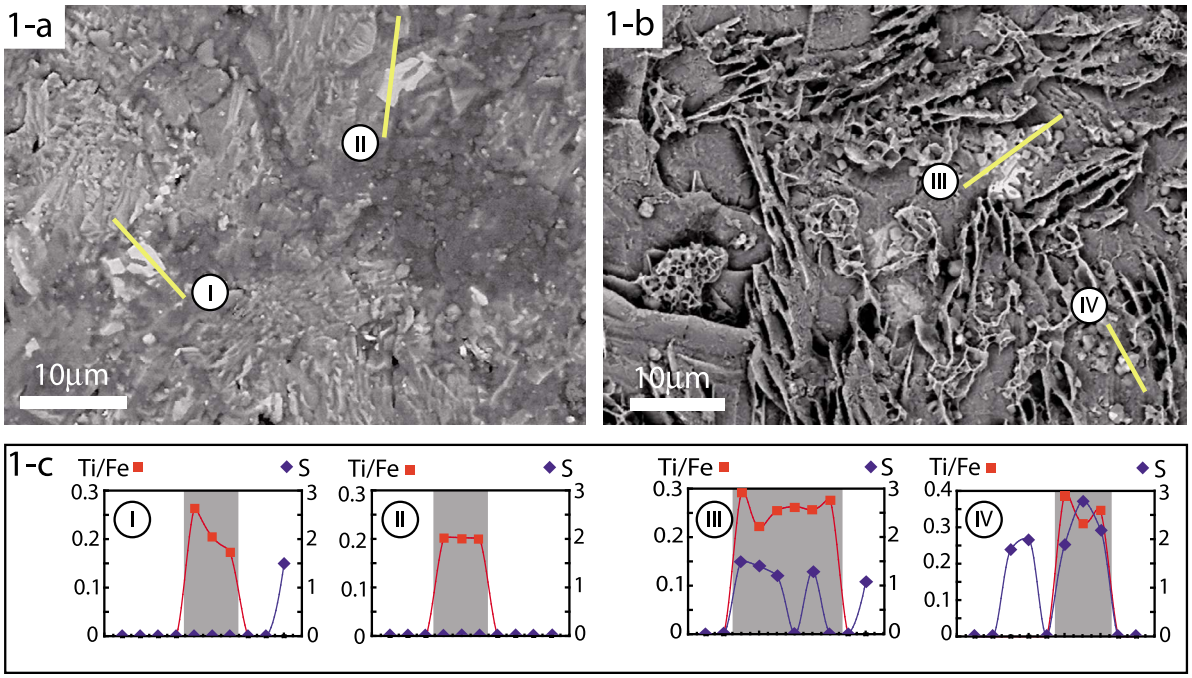

Figure 1. Scanning Electron Microscope images in backscattered mode. (a) The control sample AnF-B, batch of 10 EDSX analyses are made along two transects through two titanomagnetites apparent on the surface (light gray minerals); location of transects is indicated by yellow lines. (b) The biotic sample AnF-A, phyllosilicates are clearly visible; as in Figure 1a, location of two EDSX transects through titanomagnetites are indicated by yellow lines. (c) Semiquantitative EDSX results (using an Oxford Inca microanalysis system) obtained along the transects. Analyses are reported in atoms % and Ti/Fe between 0.2 and 0.4 are indicative of titanomagnetites (outlined by the shaded area on the diagram). Sulfur is systematically associated with titanomagnetites in the biotic sample, no such correlations are reported on the control sample.

analyses performed by SEM on titanomagnetite crystals from the control and the biotic sample (Figure 1) show that, in addition to the textural differences between the 2 samples the magnetic phases from the biotic sample were systematically associated with sulfur while this was not observed on the control sample (Figure 1c). Once again the exact phases involved and spatial relationship between elements could not be determined using this approach.

3. Method

3.1. SEM and Focused Ion Beam Milling

[8] Three ultrathin (~100 nm in thickness) foils transparent to electrons were prepared by FIB milling using the FIB "lift-out" technique (see *Heaney et al.* [2001] for details). A first FIB foil (FIB foil A, Figure 2a) was cut on sample AnF-A perpendicular to a filament using a FEI Model 200 TEM FIB system at the CP2M (University Aix-Marseille III, France). A 30 kV Ga+ beam operated at ~20 nA was used for the initial steps of the milling. Progressive excavation from both sides of the section area was performed through repeated milling of steps. Depth of milling was approximately ~7 microns. The final finest thinning of the section was made with less intense Ga^+ beam operated at 100 pA current. The section was thinner at the top (~80 nm in thickness) than at the bottom (~200 nm). The final foil measured 15 μm in length, ~6 μm in width and ~80 nm 200 nm in thickness. A line pattern was drawn with the ion beam along the side and bottom edges of the foil allowing its removal. It was finally deposited onto a carbon-coated mesh copper grid membrane using a stereomicroscope and a hydraulic micromanipulator. A second foil (FIB foil B) was cut from sample AnF-A along a filament (see Figures 2b–2d) using a Dual-FIB FEI Strata D8–235 at university Lille I (France). For this foil, a thin layer of platinum was deposited prior to milling on top of the region of interest (Figure 2c) in order to protect the top surface of sample from abrasion due to the Ga^+ beam. The same conditions as described above were used for milling and thinning. The foil measuring 20 μm *10 μm in size and 80–200 nm in thickness was directly deposited on a carbon-coated mesh copper grid using an in situ omniprobe device. Finally a third FIB foil (FIB foil C) was cut on the control sample AnF-B from a random location on the surface of the sample using a Neon Zeiss FIB at Institut de minéralogie et de physique des milieux condenses (IMPMC, Paris, France). This "control" foil showed several titanomagnetites that were subsequently analyzed by TEM.

3.2. Transmission Electron Microscopy, Scanning Transmission Electron Microscopy, and EDXS Analyses

[9] TEM observations were carried out on all foils using a Jeol 2100F microscope at IMPMC, operating at 200 kV, equipped with a field emission gun, a high resolution UHR pole piece and a Gatan energy filter GIF 200. STEM observations were performed in high angule annular dark

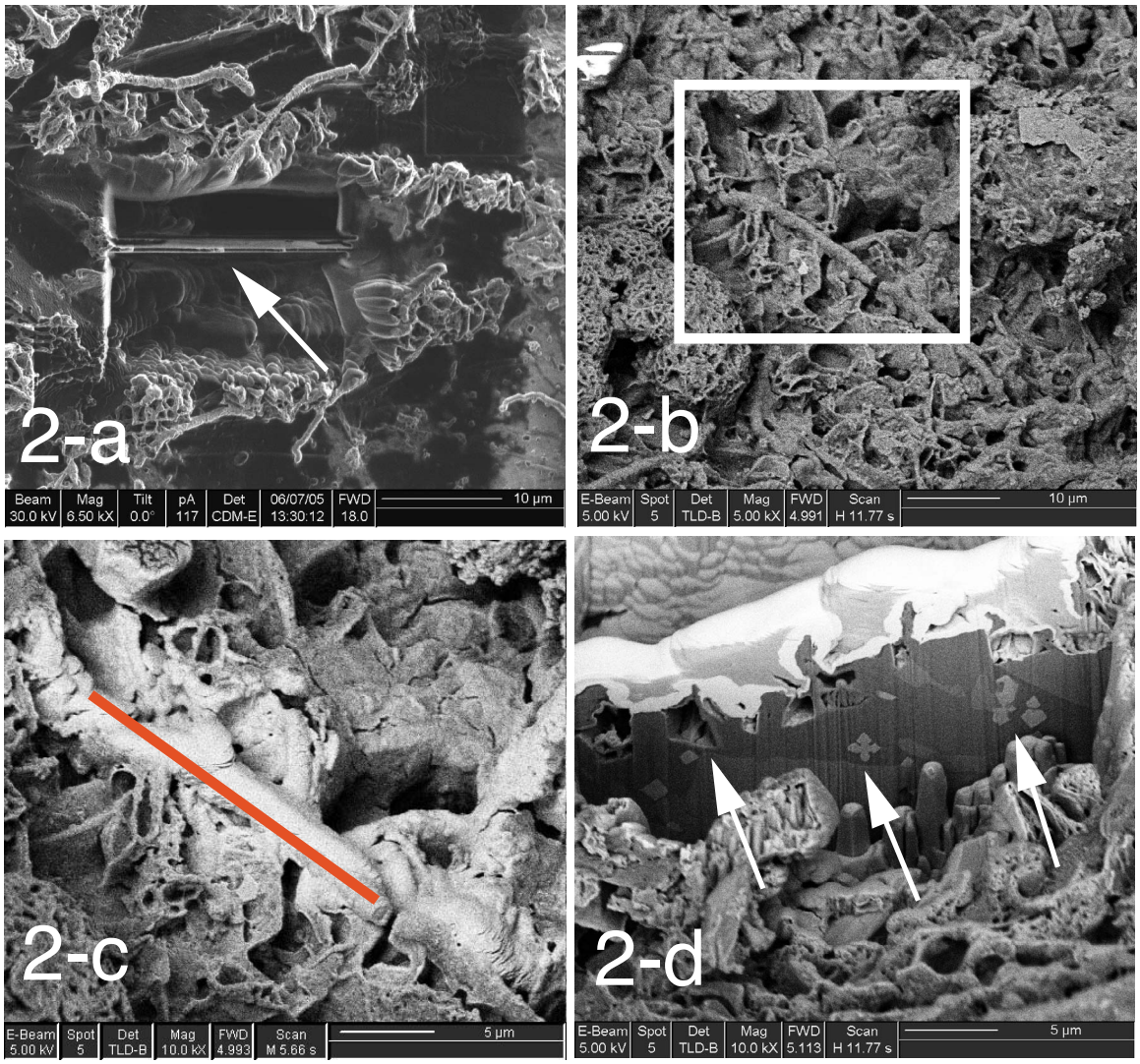

Figure 2. Scanning Electron Microscope (SEM) images and Focused Ion Beam (FIB) cross-sectioning of the filaments. (a) SEM image of the sampled area from FIB foil A; the arrow indicates the perpendicar cross section of the filaments. (b) SEM image of the selected area for FIB foil B; square corresponds to the area represented in Figure 2c. (c) Same area as Figure 2b at higher scale after the deposition of a platinum layer; the red line indicates the future position of the FIB foil. (d) FIB image of the ultrathin foil during the last thinning steps by Galium beam before the micromanipulator-assisted extraction stage; contrasts in the FIB foil chemical composition appear, and light gray crystals with dendritic morphologies can be observed (white arrows).

field mode (HAADF). Energy dispersive X-ray spectrometry (EDXS) analyses were performed using a JEOL detector with an ultrathin window that allowed detection of low-Z elements. EDXS maps were acquired in STEM HAADF mode, with a focused electron beam of a few nm.

3.3. ATEM Investigations

[10] Analytical transmission electron microscopy analyses were performed on FIB foil A at the TEM facility at Laboratoire de Structure et Propriétés de l'Etat Solide (Lille, France) on a Philips CM 30 microscope, operating at 300 kv. The TEM is equipped with an X-ray energy dispersive spectrometer (Thermo Electron Corporation, Noran Systeem equipped with Si detector and ultrathin window). The general microstructure is observed in bright field mode. Local EDXS analyses were performed using STEM mode with a probe size of 5.6 nm. The Doukhan-Van Cappellen method [*Van Cappellen and Doukhan*, 1994], based on electroneutrality of specimen was applied to have access to the local thin foil thickness and correct the analyses from thickness effects on absorption, After absorption corrections, quantitative microanalysis could be performed with a final accuracy of a few percent.

[11] A region of interest of around 2 μm^2 on FIB A foil was selected based on prior TEM observations. Regularly spaced spot analyses ranging between 30 and 50 nm in size were made within three traverses. The traverses measure from 200 to 900 nm in length. A total of 35 spot analyses were performed. For each analysis the quantification was made on iron, sulfur, silicium, titanium, aluminum and magnesium.

3.4. Scanning Transmission X-Ray Microscopy

[12] STXM observations were performed on foil A and B at the ALS branch line 11.0.2.2 following the same procedures as described in [*Bluhm et al.*, 2006]. The experimental protocols for STXM data acquisition and analysis that we used can be found in [*Hitchcock*, 2001]. A 1200 l/mm grating and 40 μm exit slit were used for carbon imaging and spectroscopy, providing a theoretical energy resolution better than 100 meV. A 1200 l/mm grating and 30 μm exit slit were used for iron imaging and spectroscopy, providing a theoretical energy resolution of 160 meV. Energy calibration was accomplished using the well resolved 3p Rydberg peak at 294.96 eV of gaseous CO_2 for the C K-edge, and the major peak of hematite at 709.5 eV for the Fe $L_{2,3}$ edges. Observations were first made at the C K-edge, then at the Fe $L_{2,3}$-edges. NEXAFS spectra were obtained by performing image stacks. Image stacks are collected by scanning the sample in the x-y direction (image stack) of selected sample areas at energy increments of 0.1 eV for carbon, and 0.15 eV for iron over the energy range of interest (280 to 310 eV for carbon, 700 to 730 eV for iron). Here, x refers to the horizontal direction, y to the vertical direction, and the x-y plane to the plane perpendicular to the X-ray beam. The stack image procedure thus consists of measuring the NEXAFS spectrum for a specific element on each pixel (one pixel can be as small as 30 nm) of the image. Counting times are of the order of few milliseconds or less per pixel. Normalization and background corrections of the Fe $L_{2,3}$-edge and C K-edge NEXAFS spectra were performed by dividing each spectrum by a second spectrum from a Fe-, or C-free location on the same sample. Enhanced contrast images were obtained by subtracting the image taken at an energy just above the absorption edge of interest from another image obtained at an energy below the absorption edge of interest.

4. Results

4.1. TEM Observations, EDXS, and ATEM Analyses

4.1.1. FIB Section A

[13] A TEM image from a portion of FIB-A foil is shown on Figure 3a. The filament (on top) is cut perpendicularly to its long axis and is lying on a rectangular-shaped plagioclase single crystal as shown by EDXS and electron diffraction analyses. Despite the difficulty of analyzing thicker areas on the foils, most of the primary silicate phases could be identified as plagioclase or pyroxene based on EDXS analyses. A poorly crystallized phase containing Si, Mg, Al, Fe, Ca (decreasing intensity order) was observed on the right hand side of the FIB foil and identified as aluminosilicates, likely smectite (data not shown). Moreover, sulfur was systematically associated with this phase, but its speciation (sulfide or sulphate) could not be determined. This phase was previously observed by SEM at the surface of the samples. In the middle of the foil, one micrometer beneath the filament, a crystal with a dendritic habitus typical of titanomagnetite shapes was observed in contact with the plagioclase (see Figure 3a). EDXS analyses and electron diffraction confirmed that this crystal is a titanomagnetite crystal. This crystal was in direct contact with the solution as shown by the presence of a porous area containing some aluminosilicates on its right side. A rim measuring 100 to 300 nm in thickness was observed around the titanomagnetite. The EDXS spectra (Figure 3b) obtained from the titanomagnetite and the surrounding rim show a significant increase of the Ti/Fe ratio as well as the presence of sulfur in the rim. Selected area electron diffraction patterns reveal additional differences between the titanomagnetite and the rim: the diffraction pattern from the titanomagnetite is indicative of a well crystallized structure, whereas the rim shows a powder electron diffraction pattern with broad arc of restricted angular stretch suggesting that it contains nanocrystalline grains with a preferential crystallographic orientation close to that of the titanomagnetite (Figure 3c). The mineralogy of the nanocrystalline grains could not be resolved as the sample was too thick for high resolution TEM. However, one possibility explaining the present data is that they are remnant nanodomains of titanomagnetite entombed in a poorly crystallized Fe-S-rich layer.

[14] In order to detail the transition from the pristine titanomagnetite to the rim, analytical EDXS quantitative analyses were performed along three lines going from the inner part of the crystal to the rim. Results are reported on Figure 3d. The titanium concentration remains fairly constant (at about 5%) in the titanomagnetite and the alteration rim. In contrast, iron shows a strong decrease (from c.a. 35% to 8–10%) at the crystal/alteration rim interface and is not uniformly distributed within the alteration rim. Sulfur is mostly localized within the alteration rim. Similar alteration rims were observed around several titanomagnetite crystals, and they were exclusively associated with titanomagnetite.

[15] The nature of the filament was difficult to determine on foil A as it was significantly damaged by FIB milling due to the lack of a platinum strap covering the sample (Figure 3a). A second foil (foil B) was thus prepared with platinum covering prior to FIB milling.

4.1.2. FIB Foil B

[16] Covering with platinum prior to FIB milling allows much better preservation of the surface of the sample and thus the investigation of the interface between the filament and the basalt. STEM observations show the filament sectioned longitudinally (Figure 4a). Some contrast heterogeneities are observed within the filament. They are associated with chemical heteorgeneities as shown by EDXS mapping

Figure 3. TEM analysis of FIB foil A (a) TEM image of FIB foil A showing the filament (on top, outlined by red dots) and the different phases within the basalt matrix (Pl, plagioclase; Phyl, phyllosilicate; Px, pyroxene; TiMt, titanomagnetite). A well crystalized titanomagnetite dendrite is observed in the middle of the photo (outlined by white dots). (b) EDX analyses and electron diffraction patterns of the titanomagnetite and surrounding alteration rim. Representative peaks in Fe, Ti, Ca, and S are seen; additional peaks of copper and galium are also visible and are attributed to a signal in the TEM chamber and the FIB milling step, respectively. (c) TEM image of the titanomagnetite and ATEM analyses made on three profiles (red lines on the photo) showing the composition variations in Fe, S, and Ti from the pristine crystal to the altered rim and down to the phyllosilicate for transect 3.

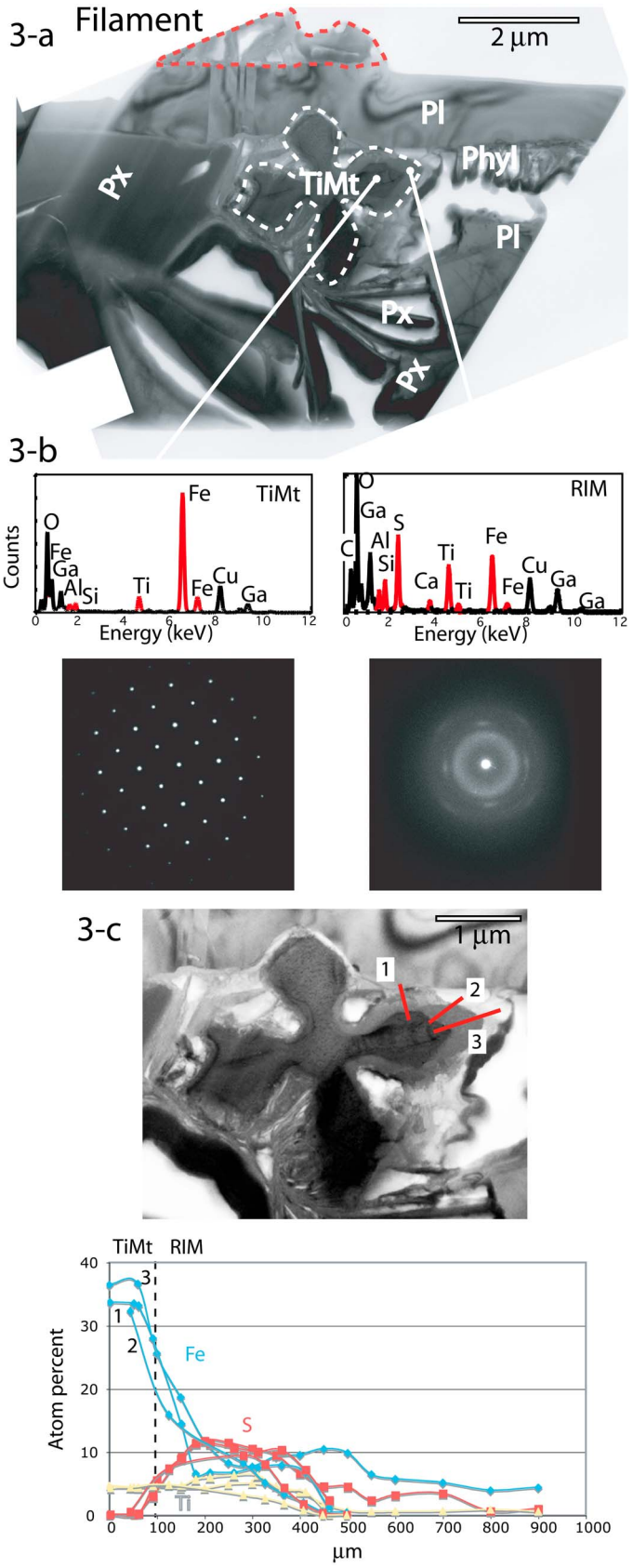
3-a
Filament
2 µm
Pl
Phyl
Px
TiMt
Pl
Px
Px
3-b
TiMt
Fe
O
Fe
Ga
Al
Si
Ti
Fe
Cu
Ga
Counts
Energy (keV)
RIM
O
Ga
S
C
Al
Si
Ti
Fe
Ca
Ti
Fe
Cu
Ga
Ga
Energy (keV)
3-c
1 µm
1
2
3
TiMt
RIM
Atom percent
Fe
S
Ti
µm

Figure 3

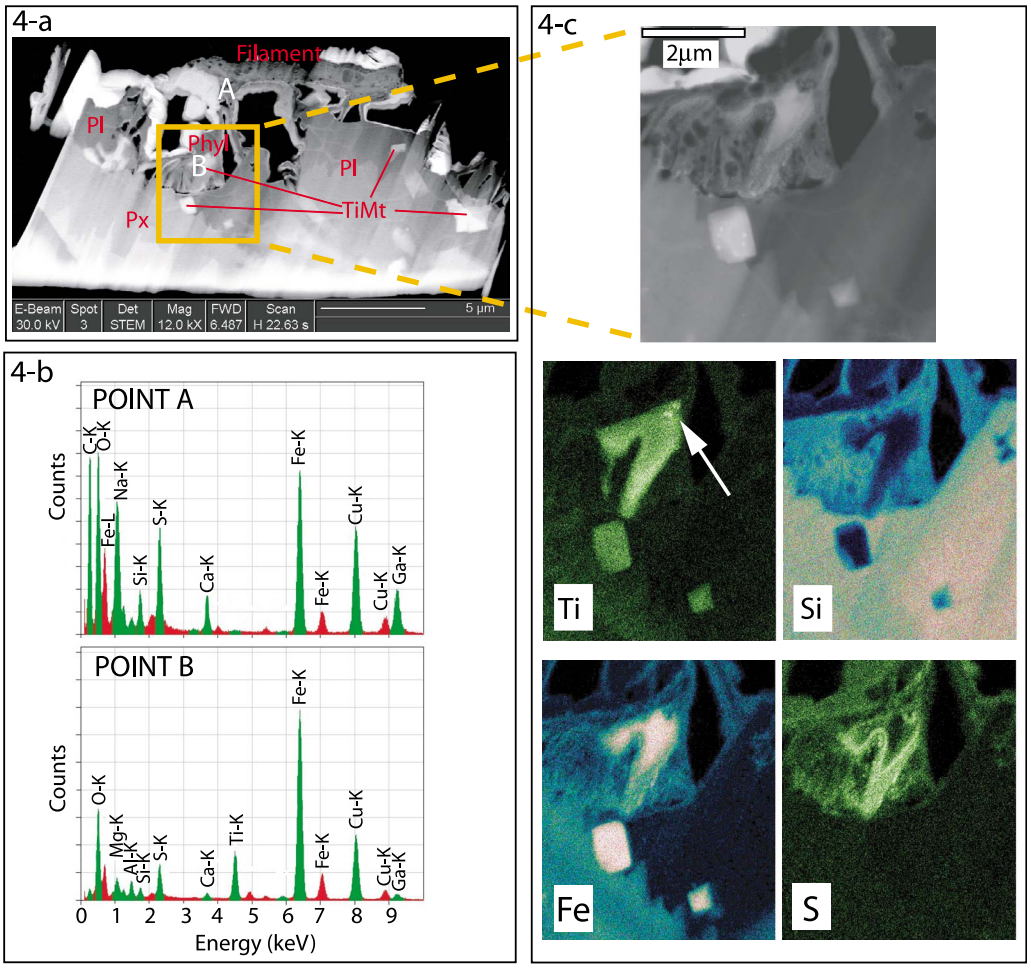

Figure 4. TEM analysis of FIB foil B (a) TEM image of FIB foil B showing the filament cut along its longer axis and the different phases within the basalt matrix. Letters A and B indicate the location of EDX analyses. (b) EDX analyses performed on point A within the microorganism, and point B within a titanomagnetite. (c) TEM image of a titanomagnetite below the filament. An alteration rim is clearly visible in the upper part of the crystal, the EDX maps of Ti, Si, Fe, and S are presented, and the white arrow indicates Ti in high concentration.

performed on the filament (Figure 4b, point A) with variable proportions of iron, sulfur and calcium at different location within the filament. A porous network with a fibrous texture is observed beneath the filament; EDXS analyses show that it is mostly composed of Si, Mg and Al with some Fe, Ca and S. This phase is chemically similar to the aluminosilicate observed in foil A. Beneath this interface, within the basalt, small titanomagnetites are observed with cubic dendritic morphologies (Figures 4a and 4b, point B). Finally, phases such as plagioclase and pyroxene are also observed. EDXS mapping was performed on an area where partly and non-weathered titanomagnetites are present (Figure 4c) revealing interesting spatial organization. Similarly to foil A, an alteration rim surrounds a titanomagnetite crystal that is adjacent to pores filled partly by aluminosilicates. The original dendritic shape of the titanomagnetite is well defined by the titanium map: the iron and sulfur maps show the extent of alteration, iron is depleted within the alteration rim, whereas sulfur is present at varying concentrations. A small (less than 100 nm wide) titanium-rich grain is seen on the uppermost part of the dendrite revealing small heterogeneity in the titanium distribution. Finally, silicon is also locally present within the iron-depleted rim around titanomagnetite.

4.1.3. FIB Foil C

[17] This FIB foil was cut in the control sample that was incubated in the culture medium but kept sterile for the whole duration of the experiment. Several titanomagnetites were observed, some in contact with the surface of the sample through pores (Figure 5a). STEM observations and EDXS mapping indicate that, in contrast to what was observed on FIB foils A (Figures 3 and 5b) and B (Figure 4), no alteration rim rich in S and depleted in Fe could be observed on magnetic phases. Sulfur was only observed in association with Fe in pyrite crystals. The absence of alteration rim within the magnetic phases and the lack of change in magnetization measured for this sample during the incubation experiment are concordant results.

4.2. STXM Analyses

[18] STXM spectromicroscopy was performed on both foils A and B at the C K-edge. Three carbon-containing areas can be discriminated on the FIB foils based on their

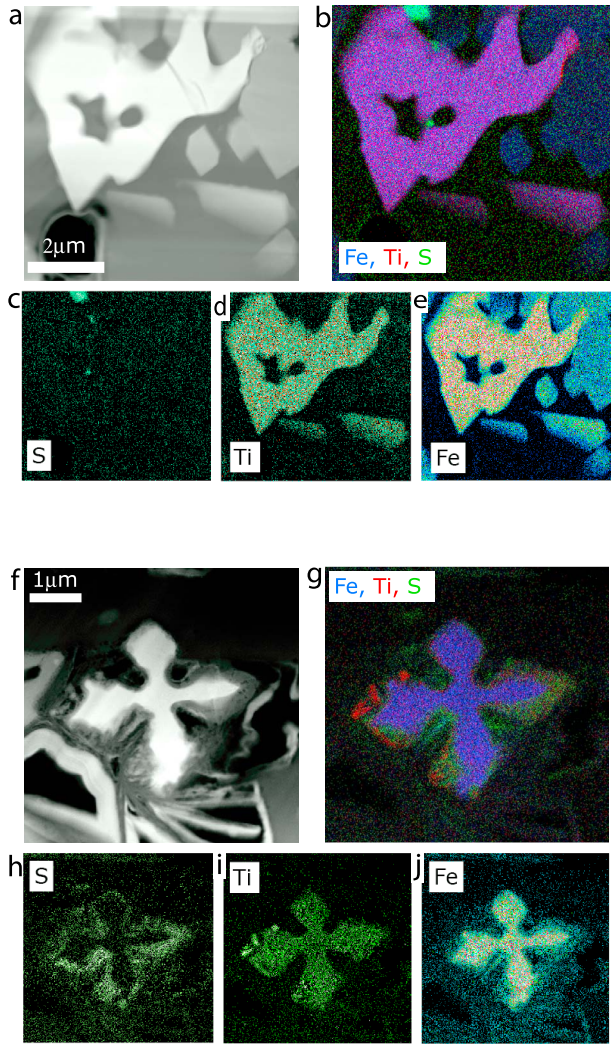

Figure 5. (a–e) TEM-EDXS mapping of nonaltered titanomagnetite in the control noninoculated sample (FIB foil C). Figure 5a shows the STEM image in HAADF mode showing one titanomagnetite in bright and two others beneath it. No alteration rim can be seen around these crystals. Figure 5b shows the overlay of the S, Ti, and Fe maps shown in Figures 5c–5e, respectively. Titanomagnetites appear in purple. No S is observed around titanomagnetites. Only S associated with Fe (without Ti) in tiny pyrite crystals can be observed. (f–j) TEM-EDXS mapping of an altered titanomagnetite from FIB foil A (outlined by white dots in Figure 3a). Figure 5f shows the STEM image in HAADF mode showing the titanomagnetite in bright and the alteration rim around it (gray). Figure 5g shows the overlay of the S, Ti, and Fe maps shown in Figures 5h–5j, respectively.

different XANES spectra and spatial distribution: the platinum strap that contains contaminating carbon resulting from the decomposition of an organometallic precursor [e.g., *Smith et al.*, 2003], the formvar composing the lacey carbon support film and finally the filaments lying at the surface of the basalt. Using spectromicroscopy, these different compounds can be easily distinguished and mapped (Figure 6). The XANES spectra measured on the filaments (Figures 6b and 6c) show major absorption peaks at (1) 284.9, (2) 286.7, (3) 288.5 which can be interpreted as 1s → π* electronic transition in (1) aromatic or olefinic, (2) ketone, and (3) carboxylic functional groups, respectively. Additionally, a peak at 290.4 eV was observed. The assignment of this peak to a particular C-functional group is more problematic. Its narrow width suggests that it corresponds to a 1s→π electronic transition, and the energy position of this peak is consistent with such an electronic transition in either carbonate, or possibly carbonyl functional groups complexing heavy elements such as Fe for example [*Chan et al.*, 2009]. Spectromicroscopy thus confirms that the filaments are mostly composed of organic carbon. On foil B, it can moreover be observed that the porous phyllosilicate beneath the filament is intimately associated with organic carbon that has the same XANES signature as in the filament suggesting that these phyllosilicates have been precipitated on some kind of extension of the filament.

[19] In parallel, indication on variations of iron speciation in the FIB foils were obtained by spectromicroscopy at the Fe $L_{2,3}$ edges. Variations in Fe speciation, including Fe redox state, can be assessed by measuring the relative intensities of absorption at 707.8 and 709.5 eV [e.g., *Miot et al.*, 2009]. Comparison between the maps of areas absorbing at 707.8 and at 709.5 eV (Figure 7) shows variations in the speciation of Fe between the different main areas of the foils. Fe is at high concentration in the organic filaments, in titanomagnetites, in pyroxenes, in aluminosilicates and in the sulfate-containing weathering rim surrounding titanomagnetites crystals. It is also present to a lower

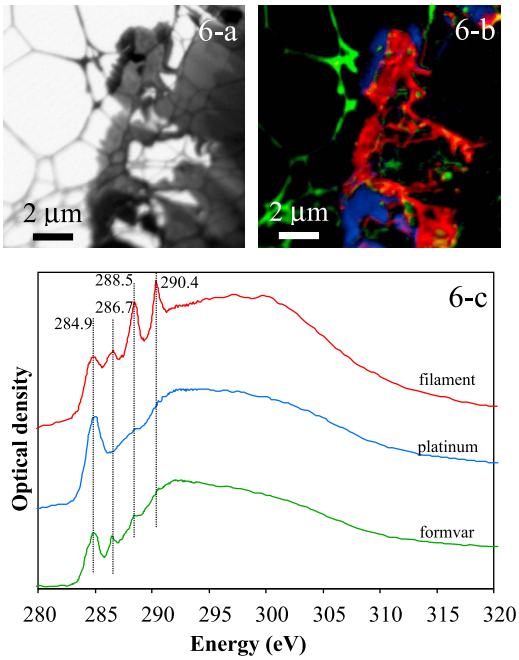

Figure 6. STXM analysis of FIB foil B at the C K-edge. (a) STXM image of the organic filament on FIB foil B at 288.7 eV. (b) Composite map obtained by overlaying the maps of carbon composing the filament (red), map comprising the platinum strap (blue) and carbon composing the lacey formvar (green). (c) NEXAFS spectra at the C K-edge of the filament, the platinum strap, and formvar.

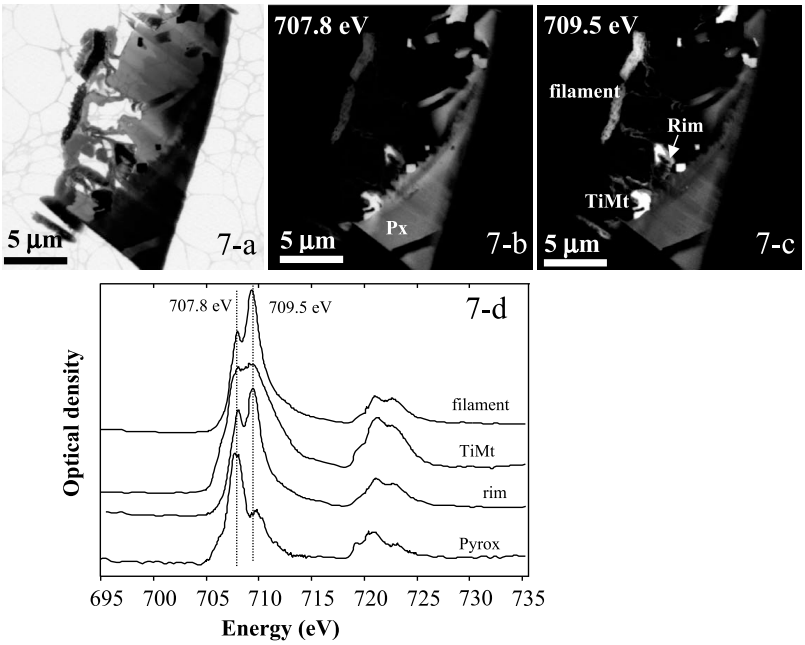

Figure 7. STXM analysis of FIB foil B at the Fe $L_{2,3}$-edge. (a) STXM image of FIB foil B at 709.5 eV. (b) Subtraction of STXM image at 707.8 eV minus image at 700 eV (below the edge) converted in OD. This difference image shows areas absorbing at 707.8 eV in bright. (c) Subtraction of STXM image at 709.5 eV minus image at 700 eV (below the edge) converted in OD. This difference image shows areas absorbing at 709.5 eV in bright. (d) NEXAFS spectra at the Fe $L_{2,3}$-edges of the filament, titanomagnetites (TiMt), pyroxenes (Px), and alteration rims around titanomagnetites (Rim).

extent in the plagioclase. Interestingly, Fe on the filament is mostly absorbing at 709.5 eV (Figure 7c) suggesting it is mostly under an oxidized Fe(III) form. Moreover, while titanomagnetites show a spectrum typical of a mixed-valence Fe phase with high absorption at both 707.8 and 709.5 eV, the weathering rim around the magnetite absorbs more at 709.5 eV suggesting that Fe is more oxidized in the rim than in the titanomagnetites. This could be due to the departure of the Fe(II) from the original titanomagnetite crystal into the solution.

5. Discussion

5.1. A Laboratory Reference of Fossil Bacteria in the Subseafloor

[20] Several recent studies have shown the pervasiveness of diverse bacterial populations within the oceanic crust [e.g., *Santelli et al.*, 2008; *Einen et al.*, 2008; *Mason et al.*, 2007; *Edwards et al.*, 2005]. The impact of these populations on the texture and chemistry of oceanic rocks is often questioned. For example, tubular microchannels have been frequently observed within oceanic glass and interpreted as a hallmark of bacterial alteration [*Furnes et al.*, 2004; *Thorseth et al.*, 2001]. However, the demonstration of the biogenicity of such structures is generally difficult to achieve [e.g., *Benzerara et al.*, 2007; *McLoughlin et al.*, 2007]. The present study offers one reference point showing how microbes interacting with basalts can look like.

[21] The origin and nature of the filaments forming at the surface of the basalts was unclear in a previous study [*Carlut et al.*, 2007]. On one hand, it was argued that they were likely of biological origin as they did not appear in noninoculated controls and they showed microbial-like morphologies. On the other hand, morphology can be a misleading criterion [*Garcia-Ruiz et al.*, 2003], and *Desulfovibrio profundus* cells do not generally show this long filamentous morphology [*Bale et al.*, 1997]. It can be noted however that filaments can occur when bacterial cells are under stress conditions and may explain the unusual morphology that is observed in the present study [e.g., *Wainwright et al.*, 1999; *Justice et al.*, 2008]. In addition, Fe-rich precipitates on similar filamentous structures, thought to be encrusted biofilm community, are reported on the surface of recent basaltic seafloor lava [*Thorseth et al.*, 2001; *Santelli et al.*, 2008]. The XANES spectroscopy analyses at the C K-edge performed in this study unambiguously show that these filaments are mostly composed of organic carbon including aromatic, ketone and carboxylic groups. Although XANES spectra of bacterial cells usually show a prominent absorption peak at 288.2 eV indicative of proteins [e.g., *Benzerara et al.*, 2006], aging of the cells and/or damages related to the FIB preparation may change this spectroscopic signature as already observed in [*Benzerara et al.*, 2005]. As a result, the filaments are likely filamentous cells of *Desulfovibrio profundus*.

[22] Those cells are heavily encrusted in minerals that contain mostly iron and sulphur. This encrustation might help preserving the organic matter over longer timescales and possibly form microfossils. These minerals also fill the interior of the cells as shown by the observation of the FIB foils. The formation of diverse minerals in association with SRB has been shown by several previous studies: for example, they can form Fe(II)-sulfates such as melanterite [e.g., *Fortin et al.*, 1996], Fe-sulfides [e.g., *Fortin and*

Beveridge, 1997] and even intracellular magnetites [e.g., *Posfai et al.*, 2006]. In the present study, the Fe- and S-rich phases were poorly crystallized or amorphous, which is a common feature in biogenic minerals [e.g., *Weiner and Dove*, 2003]. Alternatively, this may partly results from amorphization by the FIB sample preparation [e.g., *Lee et al.*, 2007]. The XANES spectra at the Fe $L_{2,3}$ edges suggest microscale heterogeneities in the Fe^{2+}/Fe^{3+} ratio associated with the different chemistries of the Fe-rich phases. While the XANES spectra of pyroxene and of magnetite are consistent with what is expected [*Benzerara et al.*, 2005], the Fe(III) composition of the phases precipitates on the filaments is intriguing regarding the anoxic conditions that prevailed during experiments and the absence of any Fe-oxidizing bacterial strain. Basalt releases Fe as Fe(II) when dissolving. Fe(II) may then combine either with sulfides or sulfates and precipitate on the cells. The presence of the oxidized form Fe (III) is thus hardly compatible with the experimental environment. Alternatively, one likely scenario is that Fe(III) form artifactually during the preparation of the samples under exposure to air. This oxidation would affect more significantly sensitive poorly crystallized phases such as those forming on microorganisms [e.g., *Miot et al.*, 2009], while Fe in more crystallized phases such as pyroxene and magnetite would keep its original redox state. The determination of the speciation of sulfur may help in a better understanding of the origin of Fe(III) and possible presence of elemental sulfur but could not be achieved by STXM. In any cases biomineralization observed on SRB filaments attests for the important quantities of iron dissolved in the solution and chemical suitability of the SRB cell surfaces for metal deposition.

5.2. Impact of Sulfate Reduction on the Composition of Basalts: Geochemical and Geophysical Significance

[23] Among the diverse metabolisms that might be of importance in the geochemical transformations of the subseafloor, sulfate reduction has been shown to be particularly relevant. Direct sampling evidences attest that SRB colonize the sedimentary column and ridge flanks [e.g., *Ravenschlag et al.*, 1999; *Huber et al.*, 2006]. But the most compelling evidence for the widespread occurrence of sulfate reduction catalyzed by microorganisms in the subseafloor comes from sulfur isotope studies. Microbial sulfate reduction causes enrichment in ^{32}S and several studies focusing on isotopic sulfur content within the sedimentary and the volcanic layers attest for the importance of SRB populations at depth [*Bottcher et al.*, 2004; *Alt et al.*, 2003]. A recent paper by [*Rouxel et al.*, 2008] is specifically related to the alteration of mid-oceanic ridge basalts and reports highly negative and heterogeneous $\Delta^{34}S$ values of late recrystallized pyrite found at a depth of up to 340 m into the basement, at site ODP 801 (western Pacific plate [*Plank et al.*, 2000]). Such negative values, attests that SRB were very active during aging of the ocean crust at this site.

[24] While our experiments are not directly comparable with the complex processes occurring in the deep sea environment, our observations could help to understand how sulfate reduction organisms can interact with some of the primary mineralogical phases inside the basalts. In our experimental study, we observed that several mineralogical transformations of basalts can be triggered, likely indirectly, by SRB. One feature is the presence of numerous aluminosilicates. It is likely that the metabolic activity of SRB by changing the chemical equilibrium of the solution, accelerate the alteration of silicates. Moreover, bacteria can provide surfaces favoring the heterogeneous nucleation of phyllosilicates [e.g., *Ueshima and Tazaki*, 2001; *Konhauser*, 1998], hence triggering secondary phase precipitation. An additional prominent feature in the present study is the alteration of titanomagnetite crystals observed in samples exposed to SRB. This provides a mineralogical basis to explain our previous observations that showed that SRB significantly weaken the magnetic signal of oceanic basalts [*Carlut et al.*, 2007]. Our observations reveal that the alteration of titanomagnetites is characterized by the formation of alteration rims around the crystals. Both foils A and B extracted from sample AnF-A show this typical alteration, while no such alteration could be observed foil C cut from the control sample AnF-B. In the two foils A and B, alteration rims around titanomagnetites systematically show similar chemical compositions (depletion in iron and enrichment in sulfur) and thicknesses. The phase (s) within the rim seems mostly amorphous with some nanodomains.

[25] Several previous studies provide a mechanistic framework for the process that likely occurs in the present experiments [e.g., *Davydov et al.*, 1998; *Poulton*, 2003; *Poulton et al.*, 2004]. Abiotic reduction of iron can be triggered at the surface of iron oxides in the presence of H_2S [e.g., *Poulton et al.*, 2004]. This process induces dissolution of iron oxides then precipitation of iron sulfides [*Yao and Millero*, 1995]. It has been shown consistently that some *Desulfovibrios* are capable of significantly catalyzing reductive dissolution of iron oxides, including magnetite [e.g., *Lovley et al.*, 1993; *Neal et al.*, 2001; *Li et al.*, 2006] by producing H_2S. Such a process could be responsible for the positive correlation with the decrease in magnetization and the metabolic activity of SRB, even so the iron oxides are not in direct contact with the bacteria cells.

6. Conclusion

[26] In this study we described how oceanic basalt samples can be affected at the nanoscale by the presence of sulfate reducing bacteria. Observation using TEM as well as EDSX and STXM allow in particular describing a specific alteration of the magnetic phases. Altered titanomagnetites are characterized by an amorphous rim composed of Fe, Ti and S. We link this specific alteration at the crystal scale to the fall of magnetization that was observed at the macroscopic scale on the same sample. We also characterized the nanoscale mineralogy of bacterial fossils at the surface of the sample. Little is known about the abundance and activity of bacterial population in the deep sea environment and such a laboratory study is not representative of the diversity and rate of reactions likely to occur. However, this contribution highlights a tentative hypothesis suggesting that metabolisms based on sulfate reduction, which are likely common in these environments, may have an impact on a major geophysical signal: the magnetic remanence carried by recent mid-oceanic ridge basalts. Our results are contributing with new data regarding biosignatures in the oceanic crust that may have been overlooked so far in the natural

environments. It would be important to perform the same kind of experiments with other mineral phases containing only Fe(II) or Fe(III) to understand the impact of such strains on the seafloor.

[27] **Acknowledgments.** We thank Christian Dominici, Christian Vanni, and Wahib Saikaly for help with the TEM FIB system from CP2M in Marseille. G. E. Brown Jr. is thanked for having provided some beamtime on the 11.0.2 STXM beamline. Tolek Tylisczak is also thanked for providing the best conditions and welcome possible on STXM beamline 11.0.2 at the ALS. The Focused Ion Beam (FIB) facility of the Institut de Minéralogie et de Physique des Milieux Condensés is supported by Région Ile de France grant SESAME 2006 I-07-593/R, INSU-CNRS, INP-CNRS, University Pierre et Marie Curie – Paris 6, and by the French National Research Agency (ANR) grant ANR-07-BLAN-0124-01. The JEOL JEM-2100F at IMPMC was supported by Region Ile-de-France grant SESAME 2000 E 1435, INSU-CNRS, INP-CNRS and University Pierre et Marie Curie – Paris 6. This work was funded by CNRS-INSU.

References

Alt, J. C., G. J. Davidson, D. A. H. Teagle, and J. A. Karson (2003), Isotopic composition of gypsum in the Macquarie Island ophiolite: Implications for the sulfur cycle and the subsurface biosphere in oceanic crust, *Geology*, *31*, 549–552.

Aubourg, C., J. P. Pozzi, D. Janots, and L. Sahraoui (2008), Imprinting chemical remanent magnetization in claystones at 95 degrees C, *Earth Planet. Sci. Lett.*, *272*, 1–2, 172–180.

Bale, S. J., K. Goodman, P. A. Rochelle, J. R. Marchesi, J. C. Fry, A. J. Weightman, and R. J. Parkes (1997), *Desulfovibrio profundus* sp nov, a novel barophilic sulfate-reducing bacterium from deep sediment layers in the Japan Sea, *Int. J. Syst. Bacteriol.*, *47*, 515–521.

Benzerara, K., T.-H. Yoon, N. Menguy, T. Tyliszczak, and G. Brown (2005), Nanoscale environments associated with bioweathering of a meteoritic Mg-Fe-Pyroxene, *Proc. Natl. Acad. Sci. U. S. A.*, *102*, 979–982.

Benzerara, K., N. Menguy, P. López-García, T. H. Yoon, J. Kazmierczak, T. Tyliszczak, F. Guyot, and G. E. Brown Jr. (2006), Nanoscale detection of organic signatures in carbonate microbialites, *Proc. Natl. Acad. Sci. U. S. A.*, *103*, 9440–9445.

Benzerara, K., N. Menguy, N. R. Banerjee, T. Tyliszczak, G. E. Brown, and F. Guyot (2007), Alteration of submarine basaltic glass from the Ontong Java Plateau: A STXM and TEM study, *Earth Planet. Sci. Lett.*, *260*(1–2), 187–200.

Bluhm, H., et al. (2006), Soft X-ray microscopy and spectroscopy at the molecular environmental science beamline at the advanced light source, *J. Electron Spectrosc. Relat. Phenom.*, *150*, 86–104.

Bottcher, M. E., B. K. Khim, A. Suzuki, M. Gehre, U. G. Wortmann, and H. J. Brumsack (2004), Microbial sulfate reduction in deep sediments of the Southwest Pacific (ODP Leg 181, Sites 1119–1125), Evidence from stable sulfur isotope fractionation and pore water modeling, *Mar. Geol.*, *205*(1–4), 249–260.

Carlut, J., and D. V. Kent (2002), Grain-size-dependent paleointensity results from very recent mid-oceanic ridge basalts, *J. Geophys. Res.*, *107*(B3), 2049, doi:10.1029/2001JB000439.

Carlut, J., H. Horen, and D. Janots (2007), Impact of microorganisms activity on the natural remanent magnetization of the young oceanic crust, *Earth Planet. Sci. Lett.*, *253*(3–4), 497–506.

Chan, C. S., S. C. Fakra, D. C. Edwards, and J. F. Banfield (2009), Iron oxyhydroxide mineralization on microbial extracellular polysaccharides, *Geochim. Cosmochim. Acta*, *73*, 3807–3818.

Coleman, M. L., D. B. Hedrick, D. R. Lovley, D. C. White, and K. Pye (1993), Reduction of Fe(III) in sediments by sulfate-reducing bacteria, *Nature*, *361*, 436–438.

Cowen, J. P., S. J. Giovanni, F. Kenig, H. P. Johnson, D. Butterfield, M. S. Rappé, M. Hutnak, and P. Lam (2003), Fluids from aging ocean crust that support macrobial life, *Science*, *299*, 120–123.

Davydov, A., K. T. Chuang, and A. R. Sanger (1998), Mechanism of H_2S oxidation by ferric oxide and hydroxide surfaces, *J. Phys. Chem. B*, *102*, 4745–4752.

Dunlop, D., and O. Ozdemir (1997), *Rock Magnetism*, 573 pp., Cambridge Univ. Press, New York.

Edwards, K. J., W. Bach, T. M. McCollom, and D. R. Rogers (2004), Neutrophilic iron-oxidizing bacteria in the ocean: Their habitats, diversity, and roles in mineral deposition, rock alteration, and biomass production in the deep-sea, *Geomicrobiol. J.*, *21*, 393–404.

Edwards, K. J., W. Bach, and T. M. McCollom (2005), Geomicrobiology in oceanography: Microbe-mineral interactions at and below the seafloor, *Trends Microbiol.*, *13*, 449–456.

Einen, J., I. H. Thorseth, and L. Ovreas (2008), Enumeration of Archaea and Bacteria in seafloor basalt using real-time quantitative PCR and fluorescence microscopy, *FEMS Microbiol. Lett.*, *282*, 182–187.

Fisk, M. R., S. J. Giovannoni, and I. H. Thorseth (1998), Alteration of oceanic volcanic glass: Textural evidence of microbial activity, *Science*, *281*, 978–980.

Fortin, D., and T. J. Beveridge (1997), Microbial sulfate reduction within sulfidic mine tailings: Formation of diagenetic Fe sulfides, *Geomicrobiol. J.*, *14*, 1–21.

Fortin, D., B. Davis, and T. J. Beveridge (1996), Role of Thiobacillus and sulfate-reducing bacteria in iron biocycling in oxic and acidic mine tailings, *FEMS Microbiol. Ecol.*, *21*(1), 11–24.

Furnes, H., N. R. Banerjee, K. Muehlenbachs, H. Staudigel, and M. de Wit (2004), Early life recorded in Archean pillow lavas, *Science*, *304*, 578–581.

Garcia-Ruiz, J. M., S. T. Hyde, A. M. Carnerup, A. G. Christy, M. J. Van Kranendonk, and N. J. Welham (2003), Self-assembled silica-carbonate structures and detection of ancient microfossils, *Science*, *302*, 1194–1197.

Heaney, P. J., E. P. Vicenzi, L. A. Giannuzzi, and K. J. T. Livi (2001), Focused ion beam milling: A method of site-specific sample extraction for microanalysis of earth and planetary materials, *Am. Mineral.*, *86*, 1094–1099.

Hitchcock, A. P. (2001), Soft X-ray spectromicroscopy of polymers and biopolymer interfaces, *J. Synchrotron Radiat.*, *8*, 66–71.

Huber, J. A., H. P. Johnson, D. A. Butterfield, and J. A. Baross (2006), Microbial life in ridge flank crustal fluids, *Environ. Microbiol.*, *8*, 88–99.

Johnson, H. P., et al. (2002), Survey studies hydrothermal circulation on the northern Juan de Fuca Ridge, *Eos Trans. AGU*, *83*, 73, 78–79.

Justice, S. S., D. A. Hunstad, L. Cegelski, and S. J. Hultgren (2008), Morphological plasticity as a bacterial survival strategy, *Nat. Rev. Microbiol.*, *6*(2), 162–168.

Konhauser, K. O. (1998), Diversity of bacterial iron mineralization, *Earth Sci. Rev.*, *43*(3–4), 91–121.

Lee, M. R., et al. (2007), Characterization of mineral surfaces using FIB and TEM: A case study of naturally weathered alkali feldspars, *Am. Mineral.*, *92*, 1383–1394.

Li, Y. L., H. Vali, J. Yang, T. J. Phelps, and C. L. Zhang (2006), Reduction of iron oxides enhanced by a sulfate-reducing bacterium and biogenic H_2S, *Geomicrobiol. J.*, *23*(2), 103–117.

Lovley, D. R., E. E. Roden, E. J. P. Phillips, and J. C. Woodward (1993), Enzymatic iron and uranium reduction by sulfate reducing bacteria, *Mar. Geol.*, *113*(1–2), 41–53.

Lysnes, K., I. H. Thorseth, B. O. Steinsbu, L. Ovreas, T. Torsvik, and R. B. Pedersen (2004), Microbial community diversity in seafloor basalt from the Arctic spreading ridges, *FEMS Microbiol. Ecol.*, *50*, 213–230.

Mason, O. U., U. Stingl, L. J. Wilhelm, M. M. Moeseneder, C. A. Di Meo-Savoie, M. R. Fisk, and S. J. Giovannoni (2007), The phylogeny of endolithic microbes associated with marine basalts, *Environ. Microbiol.*, *9*, 2539–2550.

McLoughlin, N., M. D. Brasier, D. Wacey, O. R. Green, and R. S. Perry (2007), On biogenicity criteria for endolithic microborings on early earth and beyond, *Astrobiology*, *7*, 10–26.

Miot, J., et al. (2009), Iron biomineralization by neutrophilic iron-oxidizing bacteria, *Geochim. Cosmochim. Acta*, *73*, 696–711.

Neal, A. L., S. Techkarnjanaruk, A. Dohnalkova, D. McCready, B. M. Peyton, and G. G. Geesey (2001), Iron sulfides and sulfur species produced at hematite surfaces in the presence of sulfate-reducing bacteria, *Geochim. Cosmochim. Acta*, *65*, 223–235.

Plank, T., et al. (2000), Proceedings of ODP, *Initial Rep. 185*, Ocean Drill. Program, Washington, D. C. (Available at http://www.iodp.tamu.edu/publications/185_IR/185ir.htm)

Posfai, M., B. M. Moskowitz, B. Arato, D. Schuler, C. Flies, D. Bazylinski, and R. Frankel (2006), Properties of intracellular magnetite crystals produced by Desulfovibrio magneticus strain RS-1, *Earth Planet. Sci. Lett.*, *249*, 444–455.

Poulton, S. W. (2003), Sulfide oxidation and iron dissolution kinetics during the reaction of dissolved sulfide with ferrihydrite, *Chem. Geol.*, *202*, 79–94.

Poulton, S. W., M. D. Krom, and R. Raiswell (2004), A revised scheme for the reactivity of iron (oxyhydr)oxide minerals toward dissolved sulfide, *Geochim. Cosmochim. Acta*, *68*, 3703–3715.

Ravenschlag, K., K. Sahm, J. Pernthaler, K. Sahm, and R. Amann (1999), High bacterial diversity in permanently cold marine sediments, *Appl. Environ. Microbiol.*, *65*(9), 3982–3989.

Rouxel, O., S. H. Ono, J. Alt, D. Rumble, and J. Ludden (2008), Sulfur isotope evidence for microbial sulfate reduction in altered oceanic basalts at ODP Site 801, *Earth Planet. Sci. Lett.*, *268*(1–2), 110–123.

Santelli, C. M., B. N. Orcutt, E. Banning, W. Bach, C. L. Moyer, M. L. Sogin, H. Staudigel, and K. J. Edwards (2008), Abundance and diversity of microbial life in ocean crust, *Nature*, *453*, 653–657.

Smith, S., A. J. Walton, S. Bond, A. W. S. Ross, J. T. M. Stevenson, and A. M. Gundlach (2003), Electrical characterization of platinum deposited by focused ion beam, *IEEE Trans. Semicond. Manuf.*, *16*, 199–206.

Staudigel, H., H. Furnes, N. McLoughlin, N. R. Banerjee, L. B. Connel, and A. Templeton (2008), 3.5 billion years of glass bioalteration: Volcanic rocks as a basis for microbial life?, *Earth Sci. Rev.*, *89*(3–4), 156–176.

Templeton, A. S., H. Staudigel, and B. M. Tebo (2005), Diverse Mn(II)-oxidizing bacteria isolated from submarine basalts at Loihi Seamount, *Geomicrobiol. J.*, *22*, 127–139.

Thorseth, I. H., T. Torsvik, H. Furnes, and K. Muehlenbachs (1995), Microbes play an important role in the alteration of oceanic crust, *Chem. Geol.*, *126*, 137–146.

Thorseth, I. H., T. Torsvik, V. Torsvik, F. L. Daae, and R. B. Pedersen (2001), Diversity of life in ocean floor basalt, *Earth Planet. Sci. Lett.*, *194*, 31–37.

Ueshima, M., and K. Tazaki (2001), Possible role of microbial polysaccharides in nontronite formation, *Clays Clay Miner.*, *49*(4), 292–299.

Van Cappellen, E., and J. C. Doukhan (1994), Quantitative transmission X-ray microanalysis of ionic compounds, *Ultramicroscopy*, *53*, 343–349.

Wainwright, M., L. T. Canham, K. Al-Wajeeh, and C. L. Reeves (1999), Morphological changes (including filamentation) in Escherichia coli grown under starvation conditions on silicon wafers and other surfaces, *Lett. Appl. Microbiol.*, *29*, 224–227.

Weiner, S., and P. M. Dove (2003), An overview of biomineralization processes and the problem of the vital effect, in *Biomineralization: Reviews in Mineralogy and Geochemistry*, vol. 54, edited by P. M. Dove, J. J. DeYoreo, and S. Weiner, pp. 1–29, Mineral. Soc. of Am., Chantilly, Va.

Yao, W., and F. H. Millero (1995), Oxidation of hydrogen sulfide by Mn(IV) and Fe(III) (hydr)oxides in seawater, in *Geochemical Transformations of Sedimentary Sulfur*, *ACS Symp. Ser.*, vol. 612, edited by M. A. Vairavamurthy and M. A. A. Schoonen, pp. 260–279, Am. Chem. Soc., Boston, Mass.

Zhou, H. Y., J. T. Li, X. T. Peng, J. Meng, F. P. Wang, and Y. C. Ai (2009), Microbial diversity of a sulfide black smoker in main endeavour hydrothermal vent field, Juan de Fuca Ridge, *J. Microbiol.*, *47*(3), 235–247.

A. Addad, Laboratoire de Structure et Propriétés de l'Etat Solide, UMR-CNRS 8008, Bât. C6 - Cité Scientifique, Université des Sciences et Technologies de Lille, F-59655 Villeneuve d'Ascq, France.

K. Benzerara, I. Machouk, and N. Menguy, Equipe Géobiosphère Actuelle et Primitive, UMR 7590, Institut de Minéralogie et de Physique des Milieux Condensés, CNRS, Universités Paris 6 et 7 and IPGP 140, rue de Lourmel, F-75015 Paris, France.

J. Carlut, N. Findling, and D. Janots, Laboratoire de Géologie, UMR 8538, Ecole Normale Supérieure, CNRS, 24 rue Lhomond, F-75005 Paris, France. (jcarlut@geologie.ens.fr)

H. Horen, Département de Géologie, Université de Picardie Jules Verne, F-80025 Amiens, France.